Transportation Research Part D 117 (2023) 103664

Contents lists available at ScienceDirect

Transportation Research Part D

journal homepage: www.elsevier.com/locate/trd

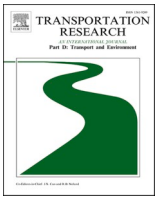

A Real-World Data-Driven approach for estimating environmental impacts of traffic accidents

Xishun Liao [a,*], Guoyuan Wu [a], Lan Yang [b], Matthew J. Barth [a]

[a] College of Engineering-Centre for Environmental Research and Technology (CE-CERT), University of California, Riverside, USA
[b] Department of Information Engineering, Chang'an University, Xi'an, Shaanxi, China

ARTICLE INFO

Keywords:
Accident impact
Energy and emissions
State prediction
Machine learning
Morphological processing

ABSTRACT

Timely and reliable accident detection provides a foundation for traffic accident management (TIM), which is critical functionality for traffic management agencies. Effective TIM strategies mitigate negative impacts caused by non-recurrent events, improve quality of service and traveler satisfaction, and enhance transportation resilience. Most existing studies focus on traffic accident detection and system mobility. Very few systems attempted to quantify the environmental impacts of accidents. We examine a cloud-based data platform that fuses information from real-world traffic, probe vehicle data, and road weather. Moreover, we developed a data-driven approach to estimate the impacts of accidents using Otsu's method, morphological operation, time-series prediction, and emissions simulator model, allowing us to quantify the benefits of advanced accident detection. The proposed method was evaluated with a real-world scenario, showing that the studied accident may cause additional energy waste by 38% and CO emissions by 36%.

1. Introduction

According to the Urban Mobility Report (Schrank et al. 2019), nearly 8.8 billion hours and 3.3 billion gallons of fuel were wasted in 2017 in the United States due to traffic congestion. In addition to *recurring* congestion factors (e.g., physical bottlenecks, fluctuations in normal traffic, disruption by control devices (Systematics, 2005)), drivers experience approximately 70 percent more travel time (compared to free-flow conditions) due to *non-recurring* inccidents. These incidents include but are not limited to unexpected traffic accidents, bad weather, temporary work zones, and special events. In this paper, we focus on traffic accidents, or more specifically motor vehicle crashes. In particular, congestion associated with traffic accidents is the most frustrating to travellers due to their unexpected and undesirable consequences (e.g., late delivery, missed flights, delayed meetings) as opposed to construction and special events, which can be avoided with alternate routes. Even worse, the presence of accidents may also lead to higher risks of secondary crashes (Dingus et al. 2016).

To mitigate these adverse impacts of traffic accidents, public agencies have initiated traffic accident management (TIM) programs and adopted a variety of strategies (Owens et al. 2010). One of the fundamental questions associated with these TIM programs or strategies is how to estimate the impacts of traffic accidents in terms of safety, mobility, and environment. Numerous methodologies have been introduced over the years to address this concern. Early studies have put significant emphasis on analytical approaches based on the queuing theory (Sullivan 1997) and shockwave analysis (Al-Deek et al. 1995). Although these approaches may address a

* Corresponding author.
E-mail address: xliao016@ucr.edu (X. Liao).

https://doi.org/10.1016/j.trd.2023.103664
Received 22 September 2022; Received in revised form 6 January 2023; Accepted 14 February 2023
Available online 8 March 2023

few interesting phenomena (e.g., "rubbernecking" effects (Teng and Masinick 2004)), they can be only applied to very limited scenarios. With the advent of traffic simulation software, especially microscopic simulation tools (e.g., VISSIM, SUMO), some researchers have proposed to use these simulation tools to model and analyze the impact of traffic accidents (Chien et al. 2002, Karioti et al. 2017). Although traffic simulation can be used to conduct "before-and-after" studies and to model a variety of "what-if" scenarios, the real-world validation of traffic flow dynamics during accidents is critical. Further, most existing studies on accident impacts have been focused on the involved vehicle(s) only or quantifying safety and mobility performance (Kumaresan 2014, Yang, et al. 2016, Du et al. 2012), while very few have considered traffic as a whole in terms of the environment.

To address the aforementioned gaps, we propose a data-driven approach to estimating the energy and emissions impacts from traffic accidents. Major contributions of this paper are:

- Built a database including real-world traffic state measurements, traffic accident records, roadway geometry, and weather information.
- Developed a data-driven method to estimate the spatial–temporal effect on traffic caused by the accident.
- Estimated the excessive energy consumption and tailpipe emissions caused by the accident.

The rest of this paper is organized as follows: Section 2 presents the integrated database built for estimating accident impacts. Section 3 details the flowchart of the proposed method and highlights the key modules: *spatiotemporal impact region identification*, *threshold determination*, *impact boundary refinement*, *accident-free traffic condition prediction*, and *energy/emissions impact estimation*. Section 4 conducts a case study with real-world data collected in Riverside, CA, followed by the concluding remarks in Section 5.

2. Construction of integrated database

In this study, several data sources are utilized to assess the accident-induced environmental impacts. As shown in Fig. 1, key information includes real-world traffic states, historical accident records, roadway geometry logs, and meteorological conditions. Regarding traffic conditions, we take advantage of the Caltrans Performance Measurement System or PeMS (https://pems.dot.ca.gov/), which receives real-time 30-second measurements of traffic count and occupancy from every loop detector throughout the California freeway system, detects invalid or missing data, and rectifies them or fills those "holes". Based on the flow and occupancy data for each lane, speed is estimated using the well-known g-factor algorithm for a single loop detector (Jia et al. 2001). In addition, all these raw data are aggregated at various temporal levels, e.g., 5 min, for different analysis purposes.

Regarding traffic accident records, the *Highway Safety Information System* or HSIS (http://www.hsisinfo.org) is considered in this study. HSIS is a multi-state (including California) database that documents safety-related information for highways. It provides not only accident inventory but also detailed information about the geometrics and other roadway characteristics, interchange ramps, and intersections, such as the number of lanes, roadway width, road surface, terrain, design speed, ramp's location, and horizontal and vertical alignment, as well as weather and lighting conditions (e.g., sunny vs cloudy). Therefore, we also use HSIS as another major data source of geometric characteristics of the freeways and weather information in addition to PeMS. In particular, HSIS may provide detailed information on traffic accidents such as the accident's lane-level location (in terms of post-mile and lane index), start time,

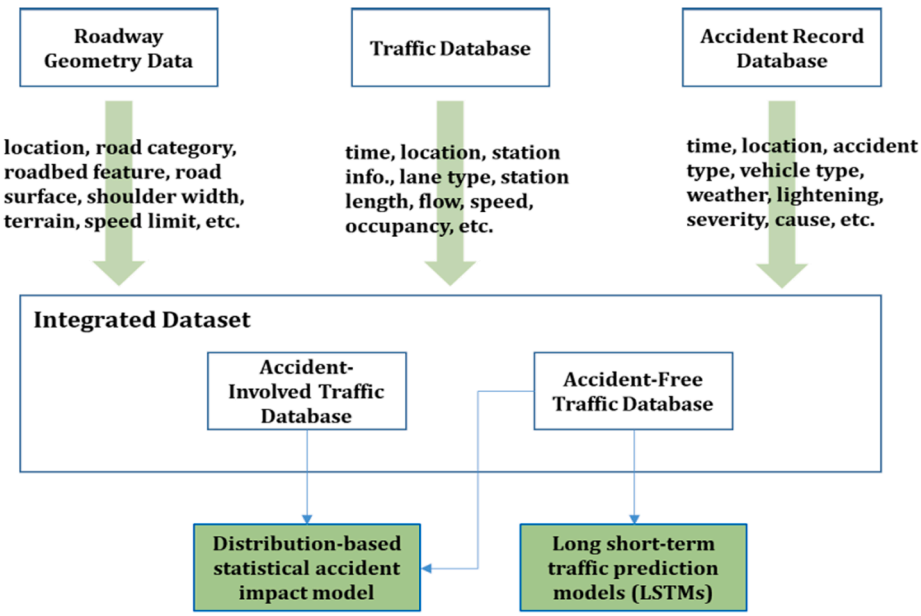

Fig. 1. Integrated database and workflow.

duration, type (e.g., rear-end, head-on, angle, and sideswipe), and severity (e.g., property damage only, numbers of involved vehicles, numbers of injuries). This information can be used to select those accidents of interest.

With the availability of all these data sources, we make a significant effort to preprocess them (e.g., inconsistency check across different sources) and develop a structured database by fusing various datasets based on the time stamp and location tags. Associated with each accident record, there are two sub-sets of traffic data in the integrated database: one includes normal traffic conditions (of multiple historical days) which are constructed by filtering out all accidents recorded in the HSIS dataset, and it is used to build the model for predicting the "accident-free" traffic states. The other is for the actual traffic condition directly related to the occurrence of an accident, i.e., the actual traffic condition after the accident, which is used to build an accident impact analysis model. These two models will be further discussed in the methodology section.

Fig. 2 illustrates the flowchart of our proposed approach to estimating the environmental impacts of traffic accidents. The orange blocks represent input data sources (from the integrated database) that enable the analysis. We first perform data fusion based on the time stamp and location tags of accidents. By associating with each accident record, we obtain two sets of traffic data: 1) a representation of normal traffic conditions without accident occurrence, which helps construct a deep learning model for predicting the "accident-free" traffic states; and 2) the actual traffic conditions with the occurrence of the accident, across a spatiotemporal region large enough to cover all of the potential impacts. Enlightened by image processing, we develop a data-driven algorithm to determine the accident-impacted area in both space and time. After identifying the impact region and predicting the traffic conditions under a "what-if" scenario (i.e., no accident), we apply the MOVESTAR (Wang et al. 2020), a U.S. Environmental Protection Agency's Motor Vehicular Emissions Simulator (MOVES) based model to conduct energy/emissions analysis. In the following, we elaborate on three key functions (see red boxes in Fig. 2) and the associated models (i.e., green blocks) in the overall workflow.

3. Methodology

3.1. Spatiotemporal impact region identification

The purpose of this module is to identify the affected area of the target accident in both time and space, so that the following energy/emissions analysis can capture the full impacts. To achieve this goal, we first construct a "baseline" spatiotemporal speed table based on available resolutions from the data. Fig. 3 presents an example of such a table where the i-th row represents the i-th road segment covered by the infrastructure-based sensor, and the j-th column represents the data collection duration starting at the j-th time stamp. For each cell in the baseline speed table, the value is determined as the p-th percentile of all speed data samples collected within that segment over multiple historical days (when no traffic accidents occurred). Therefore, the C_p-th percentile speed over D days at the i-th road segment during the j-th discrete time interval (e.g. every 5 min), denoted by $v^{pctl}(i, j)$, can be defined as:

$$Prob\left(v_d(i, j) \le v^{pctl}(i, j)\right) \ge C_p \forall d = 1, 2, \cdots, D \tag{1}$$

where $Prob(\bullet)$ represents the probability and $v_d(i, j)$ is the speed at road segment i within time window j on the d-th day. We choose the median (i.e., 50th percentile) of all speed samples across one month to represent the baseline value. This assumes that the median of

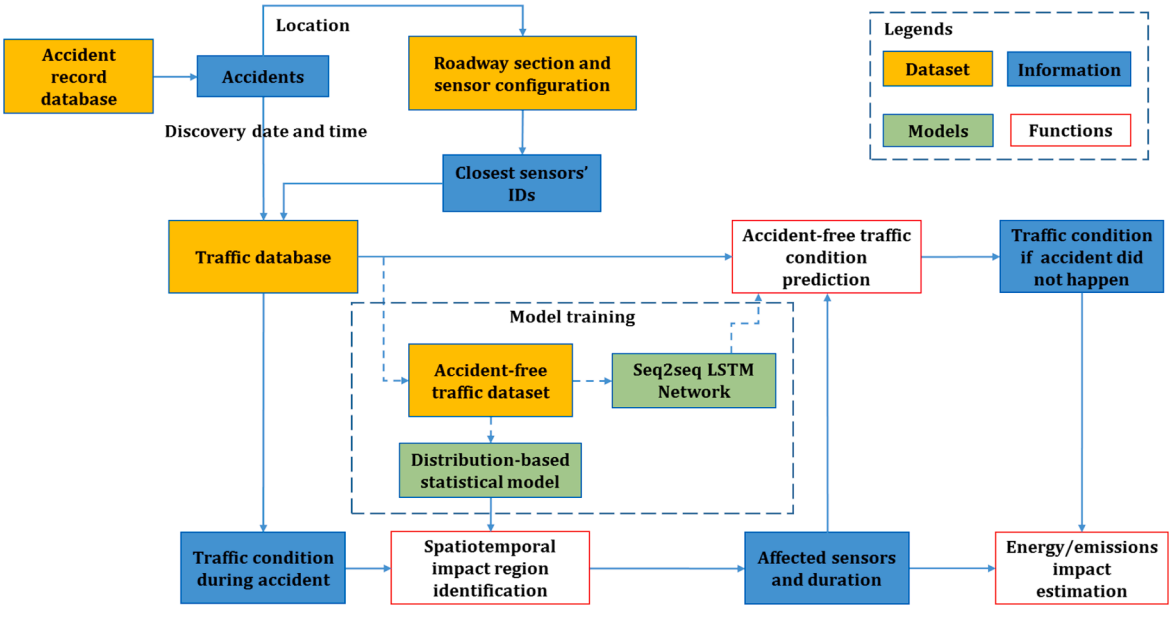

Fig. 2. Overall flowchart of our proposed methodology.

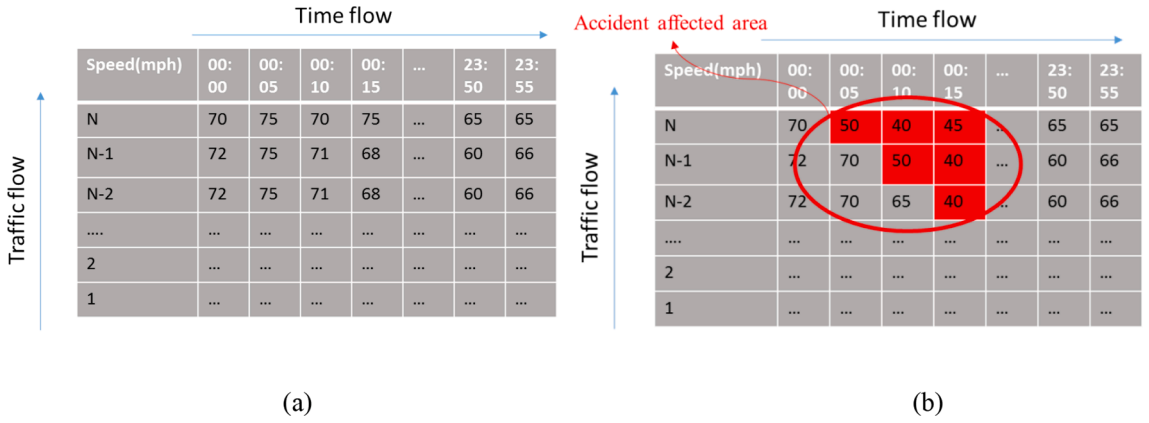

Fig. 3. An example of spatiotemporal speed tables for both baseline and accident day: (a) Baseline ("accident-free") case (b) Case with accident occurrence.

speed distributions over a time period can be representative of recurring traffic states. Non-recurrent effects if any (i.e., extreme values) would be mitigated.

By comparing the spatiotemporal speed table on the accident day (see Fig. 3(b)) with the baseline table (see Fig. 3(a)), we can flag those cells (in red) whose speeds are lower than the baseline value by certain threshold:

$$flag(i,j) = \begin{cases} 1, v^{Accident}(i,j) \le v^{Base}(i,j) - T_c \\ 0, otherwise \end{cases} \tag{2}$$

where $v^{Accident}(i,j)$ represents the speed of $cell(i,j)$ (i.e., at the i-th road segment within time window j when the accident occurs; $v^{Base}(i,j)$ is the baseline speed; and T_c denotes the threshold value to distinguish accident-affected speed and normal speed. In this study, we apply the *Otsu*'s method to determine the threshold that can maximize inter-class variance (Otsu 1979), and it is elaborated in the next subsection.

3.2. Threshold determination based on the Otsu's method

With data size increasing, manually selecting the threshold T_c becomes inefficient, also, manual methods include the human bias. As an automatic method, Otsu's Method is widely used in computer vision and image processing area to distinguish the foreground and background of a grayscale image by calculating a threshold for the intensity of the image. Similar to foreground and background, there are two classes in the study region, i.e., the affected (C_1) area and non-affected area (C_2), we can find the best threshold to distinguish the affected area from the study region by using Otsu's Method to calculate a threshold between normal speed and accident-affected speed. The first step is to calculate the speed difference between each cell of the baseline speed table (i.e., the table in Fig. 3(a)) and the speed under the accident table (i.e., the table in Fig. 3(b)):

$$\Delta v(i,j) = v^{Accident}(i,j) - v^{Base}(i,j) \tag{3}$$

Then we generate a histogram of all speed differences Δv. For the histogram of the speed difference, n_k is the number of speed difference observations that fall within bin k, and N is the total number of bins of the histogram. The speed difference histogram is normalized and regarded as a probability distribution:

$$p_k = \frac{n_k}{N}, p_k \ge 0, \sum_{k=1}^{N} p_k = 1 \tag{4}$$

The threshold T_c to separate two classes can be determined by maximizing the inter-class variance σ_B^2 of C_1 and C_2. The problem can be formulated as:

$$\max_{T_c} \sigma_B^2 = \max w_{c1}\sigma_{c1}^2 + w_{c2}\sigma_{c2}^2 \tag{5}$$

where $\sigma_{c1}^2 = (\mu_{c1} - \mu_T)^2, \sigma_{c2}^2 = (\mu_{c2} - \mu_T)^2$ are the variance of the two classes, and the weights for each class are:

$$w_{c1} = \sum_{k=1}^{t} p_k \tag{6}$$

and

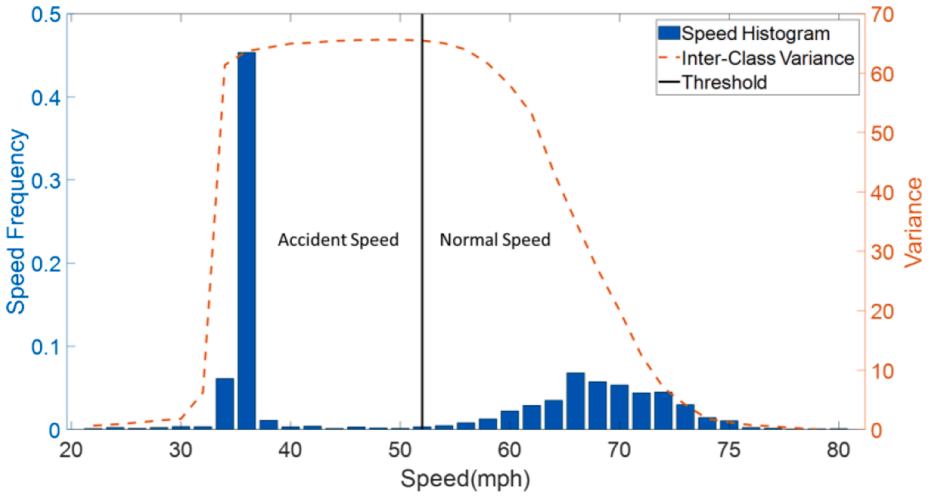

Fig. 4. An example of thresholding result using Otsu's Method.

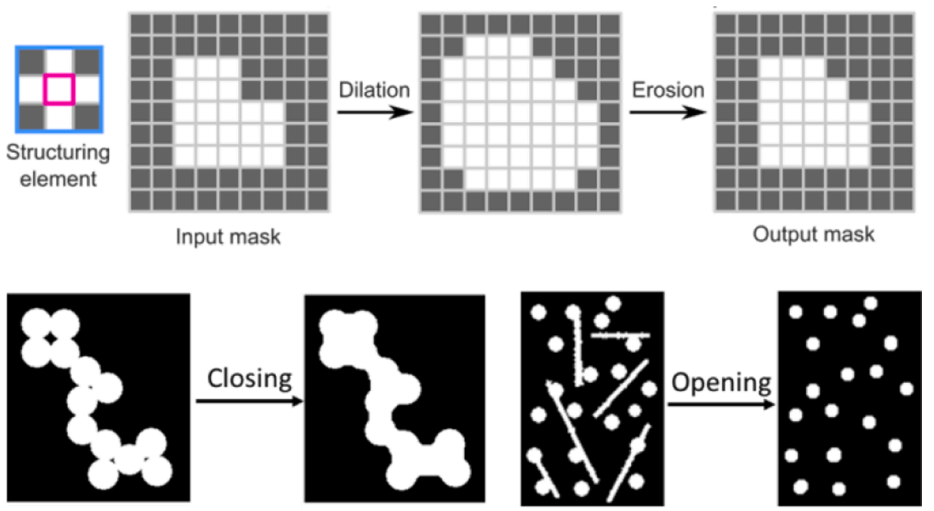

Fig. 5. Morphological operation. The closing operation is a dilation followed by an erosion, while the opening operation is an erosion followed by a dilation (Adapted from (University of Colorado Boulder, 2022)).

$$w_{c2} = \sum_{k=t+1}^{L} p_k \tag{7}$$

respectively; the mean value for each class are:

$$\mu_{c1} = \frac{1}{w_{c1}} \sum_{k=1}^{t} k p_k \tag{8}$$

and

$$\mu_{c2} = \frac{1}{w_{c2}} \sum_{k=t+1}^{L} k p_k \tag{9}$$

respectively; and the mean value for the whole table is:

$$\mu_T = w_{c1}\mu_{c1} + w_{c2}\mu_{c2} \tag{10}$$

The performance evaluation for Otsu's method for an accident is shown in Fig. 4, where a threshold (black line) is calculated to identify the accident affected area by maximizing the inter-class variance of two classes in the histogram.

3.3. Impact boundary refinement

It turns out that the threshold-based method when applied to real-world data may result in disconnected cells (Chung and Recker 2012). Considering that the progression of an accident shockwave should be (theoretically) uninterrupted, a three-layer filtering algorithm is performed on the flagged (binary) spatiotemporal speed table to guarantee continuity of the impact region. As explained in Algorithm 1, the filter consists of a noise reduction layer, a morphological closing operation layer (Van Den Boomgaard and Van Balen 1992), and a morphological opening operation layer, processing the information in such an order.

Morphological processing is a popular method to process digital images (University of Colorado Boulder, 2022) based on the shapes of objects, by applying a structuring element to an input binary or grayscale image (pixel matrix), and outputting an image that has the same size. During the process, pixels are added or removed from the object boundaries, as shown in Fig. 5. Morphological operations are used herein to trim reasonable boundaries for the accident-affected area, based on the shockwave analysis. In *Algorithm 1*, we use morphological opening and closing operations, consisting of erosion and dilation, while the former adds pixels on the object boundaries, and the latter removes pixels.

Algorithm 1: Impact Boundary Refinement

Input: 1) The raw-labelled impacted area table (*Table*); 2) A threshold (T_n) of defining noise; 3) A morphological structuring element (M_t) for temporal characteristics; 4) Morphological structuring element (M_s) for spatial characteristics.

Output: The ultimately impacted area table ($Table_{ult}$)

-Noise reduction layer-

1:Remove all connected components (objects) that have fewer than T_n cells from the binary *Table*;

-Morphological closing layer-

2:Calculate the dilation ($\oplus$) of *Table* by M_t: $Table_1 = Table \oplus M_t = \{z \in E | (M_t^s)_z \cap Table \neq \varnothing\}$, where E is a Euclidean space or an integer grid, $M_t^s = \{x \in E | -x \in M_t\}$, and $(M_t^s)_z$ is the translation of M_t^s by the vector z, i.e., $(M_t^s)_z = \{b + z | b \in M_t\}, \forall z \in E$;

3:Calculate the erosion ($\ominus$) of $Table_1$ by M_t: $Table_2 = Table_1 \ominus M_t = \{z \in E | M_{tz} \subseteq Table_1\}$, where M_{tz} is the translation of M_t by the vector z;

-Morphological opening layer-

4: Calculate the erosion of $Table_2$ by M_s : $Table_3 = Table_2 \ominus M_s$;

5: Calculate the dilation of T_3 by M_s: $Table_{ult} = Table_3 \oplus M_s$;

Considering the temporal characteristics of the shockwave, a morphological structuring element (M_t), is adopted to keep the shockwave continuous in time. For example, if the resolution of the data is 5-min, $M_t = [1 \quad 1 \quad 1]$ assumes the accident lasts at least 15 min

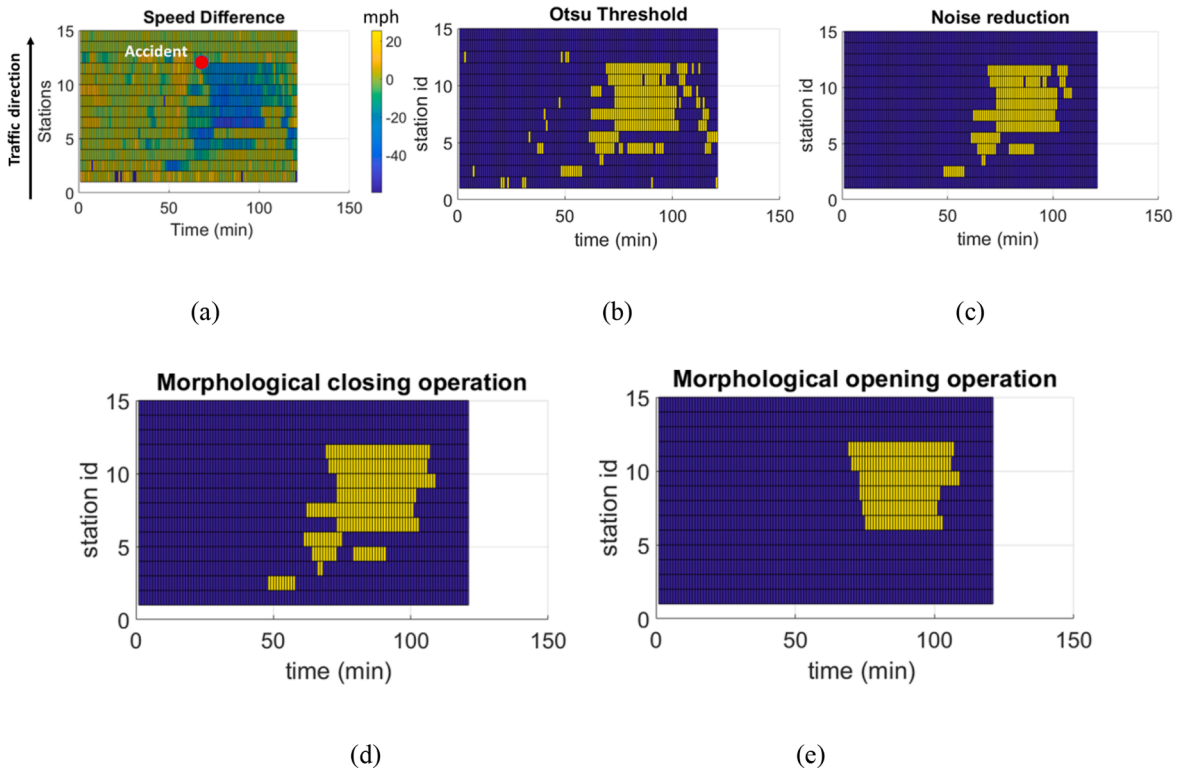

Fig. 6. Impact area evolution during the process of impact boundary refinement: (a) Speed difference map (b) raw-labelled impact area; (c) with noise reduction; (d) with the morphological closing operation; and (e) with the morphological opening operation.

(3 consecutive cells in time).

Similar to the design of M_t, a structuring element (M_s) is chosen to maintain spatial continuity. Provided that the traffic congestion or shockwave should propagate upstream along the road segment at a certain (bounded) speed, we can define M_s as an upper triangular block matrix to filter out those unreasonable noises with respect to the shockwave propagation direction. In this study, we apply

$$M_s = \begin{bmatrix} 1 & 1 & 1 \\ 0 & 1 & 1 \\ 0 & 0 & 1 \end{bmatrix} \tag{11}$$

to trim the congested cells along with the backward forming shockwave. Fig. 6 (a) visualized the table of speed differences calculated by (3), and Fig. 6 (b) shows the result of implementing Otsu's thresholding method. Fig. 6 (c) (d) (e) illustrates how the affected areas keep updating after applying each filter layer. In this case, the cell ID (standing for each station) increases along with the traffic direction, and the scanning direction of the filter matrix (e.g., M_t and M_s) is from upstream to downstream with a chronological order (i.e., from the upper left corner to the lower right corner in Fig. 6 (c) and (d)). The limitation of this method is that the morphological operations are not applied to the forward recovery shockwave, as real-world situations (e.g., re-routing of traffic) may complicate the evolution of the recovery shockwave.

3.4. Accident-Free traffic condition prediction

Once we identify the spatiotemporal region affected by an accident, we can reconstruct (predict) traffic conditions of the "what-if" scenario, i.e., assuming that the accident did not occur. Since each traffic state in the time series is highly correlated with its adjacent time steps, in this study, the Seq2seq neural network based on LSTMs (Hochreiter and Schmidhuber 1997, Kim et al. 2020) is adopted to predict "accident-free" traffic conditions, due to its capability to capture both historical traffic patterns for long-term reference and short-term information right before accident occurrence.

The data structure for the Seq2seq LSTM network is illustrated in Fig. 7, where the normal traffic dataset (without an accident) at each station over a long period (e.g., one month) is differentiated by day of the week (considering different traffic patterns for weekdays and weekends). The model is then trained for each day of the week across all the stations within the spatiotemporal impact region identified in the previous section. Fig. 8 shows the Seq2seq LSTM network structure, which consists of LSTM encoder and decoder, followed by one dropout layer to overcome overfitting; a fully connected layer with ReLU activation layer to capture the complex nonlinear pattern in the data; and an output layer. This network takes traffic measurements of a certain time window, right before the accident (based on the region described above) to predict traffic states for the next time window. The selection of the prediction window may depend on the identified temporal span due to the accident.

3.5. Energy/Emissions impact estimation

Based on 1) the actual traffic state (e.g., traffic speed) with accident occurrence; and 2) predicted traffic state with the assumption that no accident occurs, we can synthesize snippets of representative second-by-second driving cycles for each cell in the identified spatiotemporal region under two scenarios (actual vs hypothetical), and estimate the environmental performance for comparison. Constructing speed trajectories using incompleted data has been studied by many researchers (Li et al. 2020, Guo et al. 2012, Treiber and Helbing 2002). In this paper, to construct typical trajectories, we employ the default driving cycles in USEPA's MOVES database (U.S. Environmental Protection Agency 2010) differentiated with source type (e.g., passenger cars vs heavy-duty trucks), roadway type, and average speed. Table 1 lists an example to index default driving cycles in MOVES for light-duty vehicles. These driving cycles have approximate average speeds ranging from 2.5 mph to 76 mph. Note that some driving cycles may apply to freeways (in either rural or urban areas), while others are for non-freeways. In this study, we only use those driving cycles collected from urban freeway

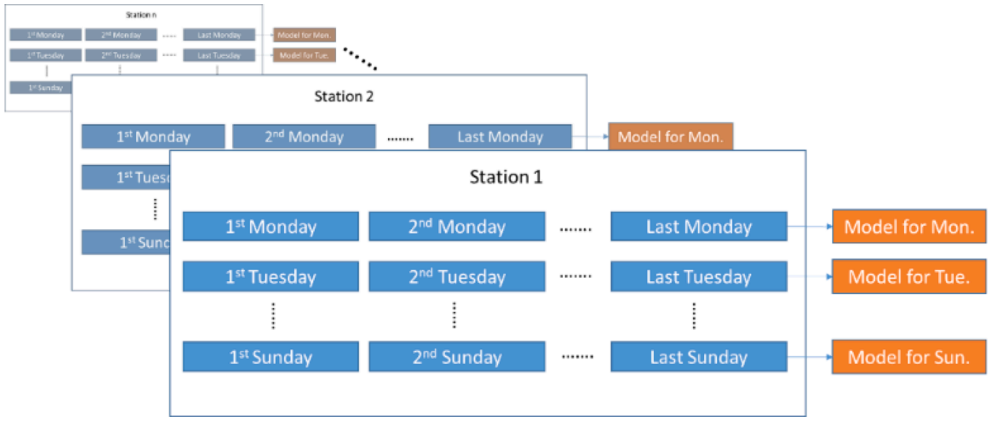

Fig. 7. Data structure of the accident-free traffic dataset.

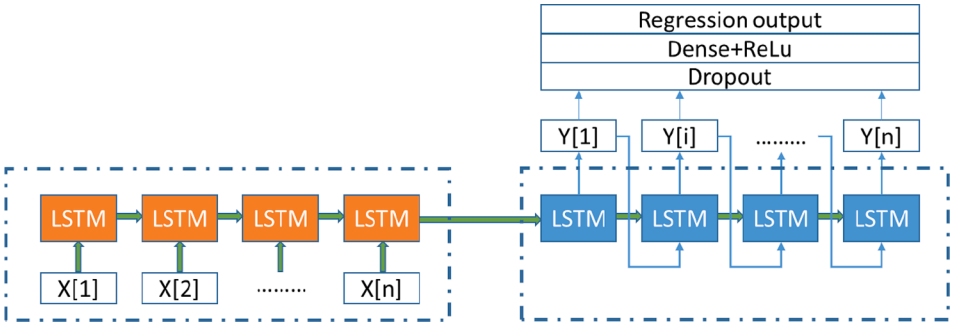

Fig. 8. The proposed Seq2seq LSTM network structure.

scenarios.

With default driving cycles in MOVES, the second-by-second representative speed trajectory for each cell can be synthesized by following these steps:

1. Select two MOVES driving cycles whose average speeds bracket the observed traffic speed at a detection station. For example, if the observed traffic speed in $cell(i,j)$ is 55 mph, then *Driving Cycle 1019* (with the average speed of 58.8 mph, as in Table 1) and *Driving Cycle 1020* (with the average speed of 46.1 mph, as in Table 1) are selected for trajectory synthesis;
2. Create speed-acceleration frequency distributions for the two selected driving cycles. In this study, bin sizes for speed and acceleration values are 2 mph and 2 mph/s, respectively;
3. Set the initial speed $v(0)$ as the observed traffic speed at detection station (e.g., 55 mph);
4. Randomly pick one of the two selected driving cycles for determining the acceleration value of the next step. The probability of choosing the target driving cycle is calculated based on how close the current speed is to the average speed of the target driving cycle. The closer these two values are, the more likely the target driving cycle would be selected. Using the same example, since$v(0) = 55$ mph, the probability of choosing *Driving Cycle 1019* is

$$p_1 = 1 - \frac{(58.8 - 55)}{(58.8 - 46.1)} = 0.7 \tag{12}$$

while the probability of choose *Driving Cycle 1020* is $1 - p_1 = 0.3$;

5. Randomly draw an acceleration value from the selected driving cycle in Step 4 and use it to calculate the speed for the next time step;
6. Repeat Step 4 and Step 5 until cumulative travel distance of the synthesized trajectory is not less than the spatial coverage of $cell(i,j)$, which is illustrated in Fig. 9.

After synthesizing the second-by-second trajectory as a representative driving cycle for each cell, we can estimate the corre-

Table 1
Moves Driving Cycle Index for Light-duty Vehicles (Adapted from (U.S. Environmental Protection Agency 2010)).

ID	Cycle Name	Average Speed	Non-Freeway		Freeway	
			Rural	Urban	Rural	Urban
101	LD Low Speed 1	2.5	X	X	X	X
1033	Final FC14LOSF	8.7			X	X
1043	Final FC19LOSAC	15.7			X	X
1041	Final FC17LOSD	18.6	X	X		
1021	Final FC11LOSF	20.6			X	X
1030	Final FC14LOSC	25.4	X	X		
153	LD LOS E Freeway	30.5			X	X
1029	Final FC14LOSB	31.0	X	X		
1026	Final FC12LOSD	20.6		X		
1020	Final FC11LOSE	46.1			X	X
1011	Final FC02LOSDF	49.1	X			
1025	Final FC12LOSE	46.1		X		
1019	Final FC11LOSD	58.8			X	X
1024	Final FC12LOSC	63.7	X	X		
1018	Final FC11LOSC	64.4			X	X
1017	Final FC11LOSB	66.4			X	X
1009	Final FC01LOSAF	73.8	X	X	X	X
158	LD High Speed Freeway 3	76.0	X	X	X	X

sponding second-by-second Vehicle Specific Power (VSP) values (in kWatt/metric ton) for the target light-duty vehicle using the equation below:

$$VSP = \frac{A \bullet v + B \bullet v^2 + C \bullet v^3 + m \bullet v \bullet (a + g \bullet \sin\theta)}{f_{scale}} \tag{13}$$

where A, B and C are road-load related coefficients for rolling resistance ($kW \bullet sec/m$), rotating resistance ($kW \bullet sec^2/m^2$), and aerodynamic drag ($kW \bullet sec^3/m^3$), respectively; m is vehicle mass (metric ton); and f_{scale} is a fixed mass factor for the source type (kg). Default values of these parameters are provided in (U.S. Environmental Protection Agency 2010). In addition, v is the target vehicle's speed (m/*sec*); a is the target vehicle's acceleration (m/sec^2); g is the gravitational acceleration (m/sec^2); and θ is the angle of road segment inclination (rad).

Once second-by-second VSP values are calculated, they are used in conjunction with speed and acceleration data to determine the corresponding operating modes according to the definition in Fig. 10 defined by MOVES. Based on the second-by-second operating modes of representative driving cycle for each cell, energy consumption and pollutant (e.g., CO, HC, NO_X, PM, and CO_2) emissions at the cell level can be estimated from the lookup tables available in MOVES database. Please note that similar procedures can be applied to heavy-duty trucks or other source types, as long as they are available in MOVES. Therefore, the overall environmental impacts due to an accident can be calculated by summing the energy consumption and pollutant emissions of all the cells within the spatiotemporal region.

4. Case study

4.1. Prediction performance evaluation

A test set from the "accident-free" traffic database is used to evaluate the performance of the LSTM models. Two prediction time windows, i.e., 30 min (6 timesteps) and 60 min (12 timesteps), are trained and tested with the same look-back and look-ahead time. The training set, validation set, and testing set are split into a ratio of 70 %, 15 %, and 15 %, respectively. The root mean square error (RMSE) of the LSTM model with 30 min prediction window is 1.3 mph for speed prediction, while the RMSE, as shown in equation (14), of the model with 60 min prediction window is 2.7 mph for speed prediction. Also, a randomly selected accident is used to present the "what-if" prediction result, as a comparison.

$$RMSE = \sqrt{\frac{\sum_{i=1}^{N} (x_i - \hat{x}_i)^2}{N}} \tag{14}$$

where x_i is the i-th value in actual data; $\hat{x}_i$ is the i-th value in predicted data; and N is the total number of the data sample.

Fig. 11 presents two examples of predicted traffic speed from the real-world data, one for a normal day and the other for an accident day. As can be observed from the figure, predicted speed (in blue) can fit actual speed (in red) very well. In particular, for the day with an accident (Fig. 11 (b)), our model is effective in predicting the hypothetical traffic speed if the accident did not occur.

4.2. Real-World accident analysis

In this section, we use real-world data to prove the efficacy of our methodology for estimating accident-related environmental impacts. The investigated accident is a rear-end one (involved with two vehicles), which occurred at 07:48:00 (PST time) on 05/16/2017 (Wednesday) along CA-91 highway in Riverside, California. The accident location is illustrated in Fig. 12. The update rate of this dataset (PeMS) is 5-minute. Following the aforementioned methodology, we obtain the speed contours for both a representative non-accident day and the accident day, and identify the continuous spatiotemporal affected region (in yellow) as shown in Fig. 13. In total, there are 39 affected cells, covering the region of 6 stations (in space) and 55 min (in time). Therefore, 6 LSTM models are trained for traffic state prediction. As shown in Fig. 14, there are two major speed drops on that day. According to the accident database, the first speed drop (during the time window between time steps 69 and 79) is caused by the accident, and the second one is recurrent traffic

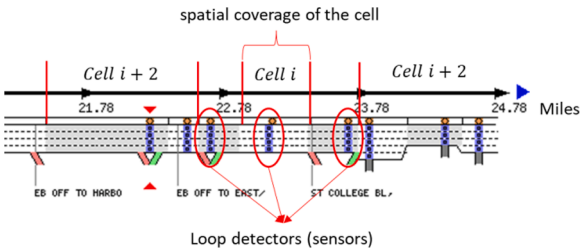

Fig. 9. Definition of cell and the spatial coverage of the cell.

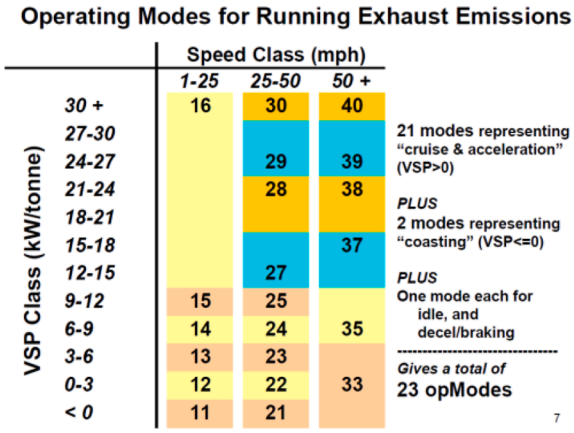

Fig. 10. Vehicle operating mode bin definition in MOVES [14].

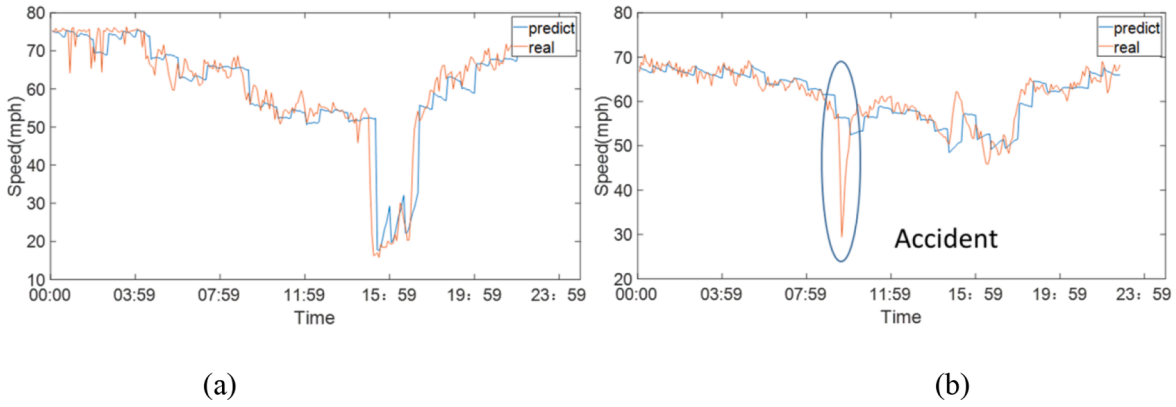

Fig. 11. Examples of traffic speed prediction using LSTM with a 60-minute prediction window. (a) Predicted traffic speed on a normal day. (b) Predicted traffic speed on an accident day.

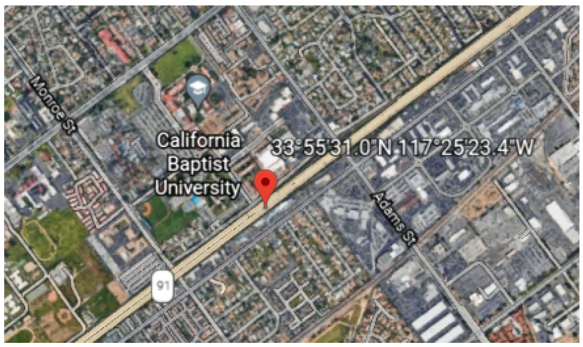

Fig. 12. Location of the accident on the Google Map (satellite image).

congestion, as recognized and predicted by the LSTM models with a 60-minute prediction window.

Following Section 3.5, we estimate the tailpipe pollutant emissions and fuel consumption using MOVES model, whose detail parameters (e.g., rolling term, rotating term, drag term, source mass and fixed mass factor) are retrieved from (US-EPA 2010). Fig. 15 shows the results for the top 20 cells whose estimated environmental impacts by the accident (i.e., the difference in fuel consumption between the actual and predicted conditions) are most significant. To obtain a realistic estimation, the fleet composition of passenger car and truck is also considered based on the truck proportion for each station from the PeMS dataset. In each affected cell, the speed of truck is estimated as 82 % of the overall traffic speed (Boriboonsomsin et al. 2011), and the energy and emissions results are calculated by weighting the volumes of passenger cars and trucks. By summing up all affected cells, the overall accident-induced environmental

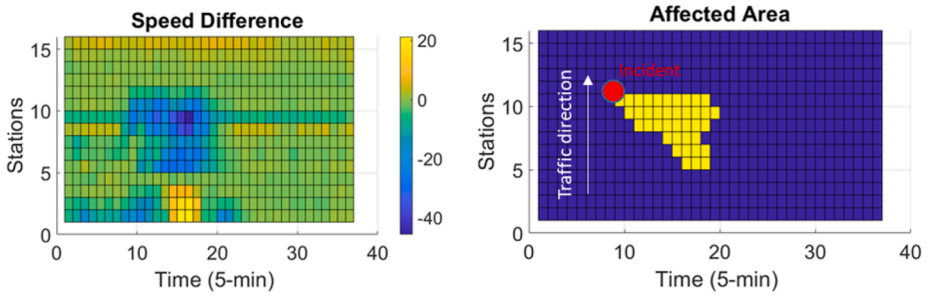

Fig. 13. Analysis of target accident affected area. (a) Speed difference contour(b) Reconstructed spatiotemporal area.

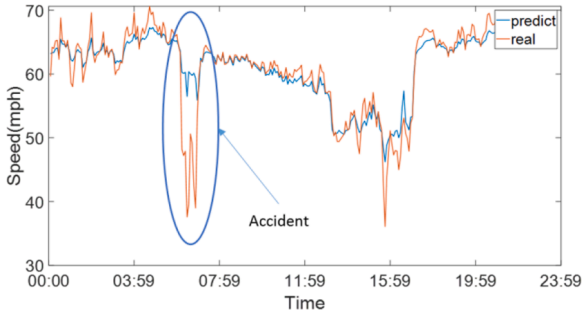

Fig. 14. Speed profile prediction result for an affected station.

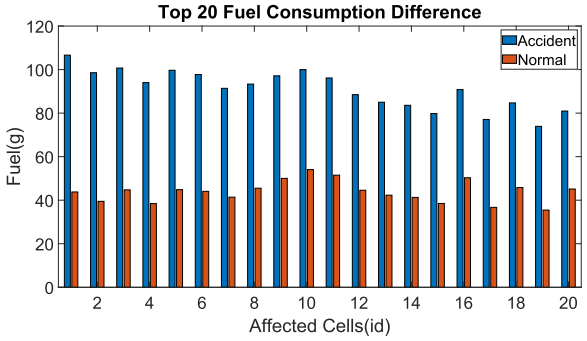

Fig. 15. Energy consumption of top 20 influenced regions due to the accident.

impacts in terms of energy consumption and pollutant emissions are summarized in Table 2.. It can be observed that if the studied accident did not happen, then energy consumption (as well as CO_2 and fuel) within the spatiotemporal impact region would be reduced by up to 38.05 % and the resultant criteria pollutant emissions (such as CO, HC, PM2.5, either elemental carbon or organic carbon) would decrease by as much as 36.47 %.

Table 2
Estimated Accident Environmental Impact of Entire Spatiotemporal Region.

	CO(g)	HC(g)	NOx(g)	PM2.5_Ele(g)	PM2.5_Org(g)	Energy(KJ)	CO2(g)	Fuel(g)
Actual (with accident)	17.74	0.16	0.83	0.009	0.06	167645.3	11927.63	3735.52
Predicted (if accident-free)	11.27	0.12	0.81	0.007	0.04	103863.1	7389.65	2314.31
Reduction (%)	36.47	25	2.41	22.22	33.33	38.05	38.05	38.05

5. Discussion

Implications. The goal of this study is to evaluate the impact of traffic accident, which consists of dataset integration, spatio-temporal impact region estimation and environmental impact analysis. These methodologies in this paper lay a solid foundation for a suite of downstream applications, including the effectiveness evaluation of various traffic accident management (TIM) strategies. For example, if a TIM strategy could reduce the duration of an accident, by either detecting the accident onset earlier or reducing the accident clearance time, the spatio-temporal impact region (as shown in Fig. 13(b)) may be mitigated based on the shockwave theory. Then, the change in environmental impact can be estimated by following the similar procedure proposed in this study.

Limitations. While this study analyses the environmental impact based on the driving cycles in MOVES, the speed trajectory synthesis approach can be improved. The proposed trajectory reconstruction for an affected cell only relies on the measurements from loop detectors, which are aggregated results from fixed locations. The data sparsity and information aggregation may limit the estimation accuracy of synthesized trajectories, thus underestimating the stop-and-go driving patterns for a congested cell. Besides the trajectory generation, the investigated accident may only reflect a portion of common accidents, and the impacts of accidents are different when other factors are considered, such as the severity of the accident, weather, and road geometry. In addition, the potential re-routing effects induced by traffic accidents, although challenging, should be further investigated and addressed in the model by estimating the fraction of directional flows based on other sources of traffic data.

6. Conclusions

In this study, we developed a methodology to estimate potential environmental impacts of traffic accident, based on real-world traffic data that may be widely available from the inductive loop detectors and archived accident data. By leveraging the integrated database, the proposed approach estimated the spatiotemporal impact region (induced by the target accident) with *Otsu*'s method and morphological operations. Once the region was determined, the Seq2seq LSTM technique was applied to historical data to predict hypothetical traffic conditions if the accident did not occur. Using both the predicted ("what-if" scenarios without an accident) and actual (scenarios with the occurrence of the target accident) traffic states, we applied the MOVESTAR model (based on USEPA's MOVES) to estimate energy/emissions impacts within the affected region (in both time and space), and estimated the differences between two scenarios, i.e., predicted vs actual. Due to the complexity in real-world traffic (e.g., re-routing) and unavailability of traffic information on the local streets, we estimated the environmental impacts based on speed variations (i.e., assuming a typical speed trajectory traversing the affected region under the "what-if" scenarios and actual scenarios). We used real-world data of an accident collected in Riverside, California to show the efficacy of our approach. The results showed that the energy consumption and tailpipe pollutant (such as CO, HC, and PM2.5) emissions could be reduced by up to 38 % and 36 %., respectively, if the target accident did not occur.

To generate more realistic speed trajectories is the one of our future steps, and data from probe vehicle can be utilized to recover the stop-and-go driving pattern. Moreover, we will evaluate the proposed method in extensive datasets by further considering other factors such as accident severity, road grade, vehicle mix, and meteorological conditions, which might aggravate the impacts (in both space and time) of traffic accidents. Unlike the current Seq2seq LSTM model that only considers the temporal correlation of each individual vehicle detection station, a more comprehensive data-driven model that can weigh the spatial correlation across all the affected stations simultaneously should be developed for better traffic state prediction.

Declaration of Competing Interest

The authors declare that they have no known competing financial interests or personal relationships that could have appeared to influence the work reported in this paper.

Acknowledgement

This study was funded by a grant from the Pacific Southwest Region University Transportation Center (UTC), supported by USDOT through the University Transportation Centers program, under Grant 69A3551747109.

The contents of this paper reflect only the views of the authors, who are responsible for the facts and the accuracy of the data presented herein. In addition, the authors are grateful for the support from HSIS staff, Anushapatel Nujjetty (FHWA) for the provision of the accident data. The authors also thank Yipeng Yang for his help on data cleaning.

References

Al-Deek, H., Garib, A., Radwan, A.E., 1995. New method for estimating freeway incident congestion. Transp. Res. Rec. 30–39.

Boriboonsomsin, K., Zhu, W., Barth, M., 2011. Statistical approach to estimating truck traffic speed and its application to emission inventory modeling. Transp. Res. Rec. 2233 (1), 110–119.

Chien, S.I.J., Goulias, D.G., Yahalom, S., Chowdhury, S.M., 2002. Simulation-based estimates of delays at freeway work zones. J. Adv. Transp. 36 (2), 131–156.

Chung, Y., Recker, W.W., 2012. A methodological approach for estimating temporal and spatial extent of delays caused by freeway accidents. IEEE Trans. Intell. Transp. Syst. 13 (3), 1454–1461.

Dingus, T.A., Guo, F., Lee, S., Antin, J.F., Perez, M., Buchanan-King, M., Hankey, J., 2016. Driver crash risk factors and prevalence evaluation using naturalistic driving data. Proc. Natl. Acad. Sci. 113 (10), 2636–2641.

Du, Y., Wu, G., Jang, K. and Chan, C.Y., 2012. Empirical Evaluation of Impacts of High-Occupancy-Vehicle Lane Collisions on Different Types of Lane Configuration in California (No. 12-4420).

Guo, W., Wang, Q., Li, Z., Tan, J., Zhang, Y., Li, L. and Zhang, Z., 2012, September. Compare linear interpolation and adaptive smoothing methods on traffic flow information reconstruction. In *2012 15th International IEEE Conference on Intelligent Transportation Systems* , pp. 1650-1655.

Hochreiter, S., Schmidhuber, J., 1997. Long short-term memory. Neural Comput. 9 (8), 1735–1780.

Jia, Z., Chen, C., Coifman, B. and Varaiya, P., 2001, August. The PeMS algorithms for accurate, real-time estimates of g-factors and speeds from single-loop detectors. In *ITSC 2001. 2001 IEEE Intelligent Transportation Systems. Proceedings (Cat. No. 01TH8585)* (pp. 536-541). IEEE.

Karioti, E., Basbas, S., Mintsis, E., Mintsis, G., Taxiltaris, C., 2017. Traffic and environmental impacts of traffic incidents on Thessaloniki's inner ring road. Transp. Res. Procedia 24, 288–295.

Kim, W., Han, Y., Kim, K.J., Song, K.W., 2020. Electricity load forecasting using advanced feature selection and optimal deep learning model for the variable refrigerant flow systems. Energy Rep. 6, 2604–2618.

Kumaresan, V., 2014. Modeling of short term and long term impacts of freeway traffic incidents using historical data. University of Nevada, Las Vegas. Ph. D. Thesis,.

Li, L., Jiang, R., He, Z., Chen, X.M., Zhou, X., 2020. Trajectory data-based traffic flow studies: A revisit. Trans. Res. Part C: Emerging Technol. 114, 225–240.

Otsu, N., 1979. A threshold selection method from gray-level histograms. IEEE Trans. Syst. Man Cybern. 9 (1), 62–66.

Owens, N., Armstrong, A., Sullivan, P., Mitchell, C., Newton, D., Brewster, R. and Trego, T., 2010. *Traffic incident management handbook* (No. FHWA-HOP-10-013).

Schrank, D., Eisele, B. and Lomax, T., 2019. Urban mobility report 2019.

Sullivan, E.C., 1997. New model for predicting freeway accidents and accident delays. J. Transp. Eng. 123 (4), 267–275.

Systematics, C., 2005. *Traffic congestion and reliability: Trends and advanced strategies for congestion mitigation* (No. FHWA-HOP-05-064). United States. Federal Highway Administration.

Teng, H. and Masinick, J.P., 2004. *An analysis on the impact of rubbernecking on urban freeway traffic* (No. UVACTS-15-0-62). University of Virginia. Center for Transportation Studies.

Treiber, M. and Helbing, D., 2002. Reconstructing the spatio-temporal traffic dynamics from stationary detector data. Cooper@ tive Tr@ nsport@ tion Dyn@ mics, 1 (3), pp.3-1.

U.S. Environmental Protection Agency, 2010. MOVES2010 Highway Vehicle Population and Activity Data. Report No. EPA-420-R-10-026, Ann Arbor, MI.

US-EPA, 2010. MOVES2010 Highway vehicle population and activity data. EPA-420-R-10-026.

University of Colorado Boulder, 2022. Morphological opening and closing: Getting Started with Image Analysis. (n.d.). URL https://canvas.colorado.edu/courses/61439/pages/morphological-opening-and-closing/ (accessed 09.12.2022).

Van Den Boomgaard, R., Van Balen, R., 1992. Methods for fast morphological image transforms using bitmapped binary images. *CVGIP*. Graphical Models and Image Processing 54 (3), 252–258.

Wang, Z., Wu, G. and Scora, G., 2020. MOVESTAR: An open-source vehicle fuel and emission model based on USEPA MOVES. *arXiv preprint arXiv:2008.04986*.

Yang, et al., 2016. Development of an Automated Approach for Quantifying Spatiotemporal Impact of Traffic Accidents. *Proceedings of 95th TRB Annual Meeting*, Washington D.C.